

Crust Cooling Models are Insensitive to the Crust-Core Transition Pressure for Realistic Equations of State

SUDHANVA LALIT,^{1,*} ZACH MEISEL,^{1,*} AND EDWARD F. BROWN^{2,3,*}

¹*Institute of Nuclear & Particle Physics, Department of Physics & Astronomy, Ohio University, Athens, Ohio 45701, USA*

²*Department of Physics & Astronomy, Michigan State University, East Lansing, Michigan 48824, USA*

³*Department of Computational Science, Mathematics, & Engineering, Michigan State University, East Lansing, Michigan 48824, USA*

ABSTRACT

Neutron stars cooling after sustained accretion outbursts provide unique information about the neutron star crust and underlying dense matter. Comparisons between astronomical observations of these cooling transients and model calculations of neutron star crust cooling have frequently been used to constrain neutron star properties such as the mass, radius, crust composition, and presence of nuclear pasta. These calculations often use a fixed pressure at which the crust-core transition happens, though this quantity depends on the dense matter equation of state. We demonstrate that varying the crust-core transition pressure in a manner consistent with adopting various equations of state results in modest changes to the crust cooling light curve. This validates the approach adopted in most crust cooling studies to date, where the neutron star mass and radius are varied while leaving the crust-core transition pressure constant.

Keywords: stars: neutron, equation of state

1. INTRODUCTION

Neutron stars cooling after sustained accretion outbursts are a significant class of observables used to probe the structure of neutron stars and thereby the behavior of ultradense matter (Wijnands et al. 2017; Meisel et al. 2018; Baym et al. 2018). The light curves from these cooling transients are often interpreted by modeling the thermal relaxation of the neutron star crust once accretion-driven heating ceases (Brown et al. 1998; Ushomirsky & Rutledge 2001; Colpi et al. 2001; Rutledge et al. 2002; Shternin et al. 2007; Brown & Cumming 2009; Page & Reddy 2013). To date, a number of studies (see, e.g., Degenaar et al. 2014; Deibel et al. 2015; Merritt et al. 2016; Waterhouse et al. 2016; Meisel & Deibel 2017; Parikh et al. 2017; Ootes et al. 2018; Parikh et al. 2018) have employed such model-observation comparisons to constrain several neutron star properties, such as the mass M , radius R , crust composition, accretion history, thermal structure, and presence of nuclear pasta.

A major feature of the accreted crust composition is the impurity, defined by the parameter $Q_{\text{imp}} \equiv n_{\text{ion}}^{-1} \sum_j n_j (Z_j - \langle Z \rangle)^2$, where Z_j is the nuclear charge of species j , with average $\langle Z \rangle$, and the number density of ions n_{ion} and species n_j , respectively. Q_{imp} quantifies the thermal conductivity of the

neutron star crust, which is dominated by electron-impurity scattering for the majority of the crust (Itoh & Kohyama 1993). Generally, model-observation comparisons for cooling transients have determined that crusts are relatively pure, i.e. Q_{imp} is relatively small. For example, $Q_{\text{imp}} \approx 3-4$ for XTE J1701-462 (Page & Reddy 2013), $4.4_{-0.5}^{+2.2}$ for KS 1731-26 (Merritt et al. 2016), $\lesssim 6$ for MXB 1659-29 (Parikh et al. 2018), and is ~ 1 for Swift J174805.3244637 (Degenaar et al. 2015), Aql X1 (Waterhouse et al. 2016), 1RXS J180408.9-342058 (Parikh et al. 2018), and MAXI J0556-332 (though Q_{imp} is not particularly relevant for such a hot crust; Deibel et al. 2015). Two significant exceptions (aside from cases considering substantial light-element enhancement in the neutron star ocean; Medin & Cumming 2014) are EXO 0748-676 with $Q_{\text{imp}} = 40$ (Degenaar et al. 2014)¹ and IGR J17480-2446 with $Q_{\text{imp}} > 25$ (Vats et al. 2018)².

However, Q_{imp} determinations from crust cooling model-observation comparisons are sensitive to other assumptions about the neutron star crust. The time for heat to diffuse from a column depth $y \equiv \int_r^\infty \rho dr'$ to the neutron star surface is

¹ Turlione et al. (2015) used $Q_{\text{imp}} = 1$ to fit EXO 0748-676; however, those authors fixed the atmosphere temperature during accretion rather than letting the temperature be determined by accretion-related heating.

² Reaction network calculations (Lau et al. 2018) find a larger Q_{imp} in the accreted outer crust; in this region, however, electron-ion scattering dominates and impurity scattering is not as important (Brown & Cumming 2009).

(Henyey & L’Ecuyer 1969; Brown & Cumming 2009)

$$\tau = \frac{1+z}{4} \left[\int_0^y \left(\frac{C_P}{\rho K} \right)^{1/2} dy' \right]^2, \quad (1)$$

where $1+z = 1/\sqrt{1-2GM/(Rc^2)}$ is the surface gravitational redshift, with c being the speed of light and G the gravitational constant. Here C_P is the specific heat per unit mass at constant pressure, ρ is the mass density, and K is the thermal conductivity. For the inner crust, $K \propto Q_{\text{imp}}$ (see Brown & Cumming 2009, and references therein) and C_P depends sensitively on the composition and whether or not the neutrons in the inner crust are paired (see the discussion in Meisel et al. 2018). M and R enter into τ through the integral over column y and through the redshift $1+z$.

Thermal gradients in the crust determine which direction heat diffuses. After accretion ceases, heat will flow from the location of accretion-powered heat sources to cooler regions at deeper and shallower depths. Predominant heating sources include the unknown source of shallow heating required to match observed cooling curves (Brown & Cumming 2009; Deibel et al. 2015), electron captures in the ocean and crust (Gupta et al. 2007), and deep crustal heating associated with neutron emissions and pycnonuclear fusion (Steiner 2012). As shallow heating tends to dwarf electron-capture heating, the latter is typically absorbed by the former in model calculations.

In reproducing observed transient light curves, which essentially requires reproducing $\tau(y)$, calculations often vary M , R , and Q_{imp} , along with properties mostly related to accretion. The crust-core transition pressure and the crust EOS is generally held fixed when fitting the lightcurve (see, e.g., Brown & Cumming 2009; Deibel et al. 2015; Merritt et al. 2016), so that the crust thickness Δr varies only through the dependence on M and R . Upon expanding the Tolman-Oppenheimer-Volkoff (TOV) equation in $\Delta r/R$, one finds that to first order, Δr is related to M and R by (Zdunik et al. 2017; Sotani et al. 2017)

$$\Delta r \approx \chi \frac{R^2}{GM} \left(1 - \frac{2GM}{Rc^2} \right), \quad (2)$$

where $\chi = \int dP/(\rho+P/c^2)$ depends only on the crust equation of state (EoS) and is integrated from the crust-core transition pressure to the photosphere. Equation (2) is analogous to the Newtonian expression for the thickness of a thin atmosphere, $\Delta r \approx PR^2/(GM\rho)$. Since varying M and R independently is equivalent to changing the dense matter EoS, the factor χ should in principle also vary. Moreover, the thickness of the crust is sensitive to the assumed pressure of the crust-core transition, and many (e.g., Steiner et al. 2015; Tsaloukidis et al. 2019) have speculated that there should be a corresponding impact on the crust cooling. In this work we

explore the impact of the EoS modification to Δr on light curves of cooling transient neutron stars.

In Section 2 we discuss the connection between Δr and the EoS. We then model cooling transient light curves in Section 3, highlighting the individual impact of changes in Δr for a variety of model assumptions. Section 4 explains the insensitivity of model calculation results to changes in Δr and the implications for the extraction of neutron star properties from model-observation comparisons.

2. THE EQUATION OF STATE AND THE CRUST THICKNESS

The dense matter EoS provides the pressure-baryon density relation $P(n)$ needed to evaluate the TOV equations (Oppenheimer & Volkoff 1939; Tolman 1939) of general relativistic hydrostatic equilibrium for neutron star structure. At present, the EoS is insufficiently constrained, leading to a variety of predictions for neutron star properties (see Lattimer 2012; Lattimer & Prakash 2016; Özel & Freire 2016; Lalit et al. 2019, for recent discussions).

Near nuclear saturation density n_s , the energy per nucleon may be written (see, e.g., Horowitz et al. 2014) as $\mathcal{E}(n, \alpha) = \mathcal{E}(n, \alpha = 0) + S(n)\alpha^2$, where $\alpha = (n_n - n_p)/(n_n + n_p)$ is the neutron-proton asymmetry. Here $\mathcal{E}(n, \alpha = 0)$ is the energy per nucleon of neutron-proton symmetric matter, and the quantity $S(n)$ is the nuclear symmetry energy, which is often expressed in an expansion about n_s :

$$S(n) = J + \frac{n - n_s}{3n_s} L + \dots \quad (3)$$

In this expression, $J \equiv S(n = n_s)$ and

$$L = 3n_s \left(\frac{\partial S}{\partial n} \right) \Big|_{n=n_s}. \quad (4)$$

At $n = n_s$, the energy of symmetric matter is minimized, i.e., $\partial \mathcal{E}(n, \alpha = 0)/\partial n|_{n=n_s} = 0$; as a result, the pressure of pure neutron matter near saturation is $P(n, \alpha = 1) = n^2 L/(3n_s)$.

The EoS determines Δr by setting the baryon density at which the crust-core transition occurs, n_t . This density is approximately given by (Newton et al. 2013; Steiner et al. 2015)

$$n_t = S_{30}(0.1327 - 0.0898L_{70} + 0.0228L_{70}^2) \text{ fm}^{-3}, \quad (5)$$

Table 1. Important EoS properties for this work.

	SLY4	APR	BL	GM1
S [MeV]	32.0	32.6	35.4	32.5
L [MeV]	46.0	57.6	76.0	94.0
n_t [fm^{-3}]	0.0892	0.0807	0.0732	0.0577
$\log_{10}(P_t/[\text{g cm}^{-1} \text{ s}^{-2}])$	32.9	32.8	32.7	32.5
$R_{1.4}$ [km]	11.7	11.3	12.3	13.8
$R_{2.0}$ [km]	10.7	10.8	11.2	13.4

where $S_{30} \equiv S/(30 \text{ MeV})$ and $L_{70} \equiv L/(70 \text{ MeV})$. This correlation is determined both by fits to nuclear experiments and theoretical calculations of pure neutron matter. Using Equation (5), the pressure at the base of the crust can be evaluated from an EoS as $P_t \equiv P(n_t)$. This quantity is more useful than n_t since P is continuous throughout the crust and is therefore commonly used as a coordinate for depth.

To explore the impact of the EoS on neutron star crust cooling, we have made a selection of nucleonic EoS that have a maximum neutron star mass $> 2 M_\odot$, so as to match observed pulsars (Demorest et al. 2010; Antoniadis et al. 2013). In order to sample some of the EoS phase space, we use the Skyrme EoS calculated with the SLY4 effective interaction (Gulminelli & Raduta 2015; Chabanat et al. 1998), the microscopic EoS APR (Akmal et al. 1998), the microscopic EoS BL (Bombaci, Ignazio & Logoteta, Domenico 2018), and the relativistic mean field EoS GM1 (Glendenning & Moszkowski 1991), where key quantities for this work are listed in Table 1. The microscopic EoS are calculations using different nucleon-nucleon interactions and three-body forces. The latter three EoS have an inner crust described using SLY4 (Douchin & Haensel 2001). Note that the procedure for matching between this and the core EoS can impact R and Δr (Fortin et al. 2016). However, our purpose is to sample a variety of n_t - M - R combinations and so the exact R and Δr are not important. Furthermore, the impact of the crust EoS on R and Δr can be nearly eliminated using the recently developed method of Zdunik et al. (2017).

3. CRUST COOLING CALCULATIONS

Cooling transient light curves were calculated using the open-source code `dStar` (Brown 2015). `dStar` models the thermal evolution of a neutron star crust after an extended accretion outburst by solving the general relativistic heat diffusion equation using the MESA (Paxton et al. 2011, 2013, 2015, 2018) numerical libraries. The microphysics is detailed in Brown & Cumming (2009). A number of thermodynamic, composition, structural, and numerical controls are available. Here we largely use a fixed set of conditions and explore the impact of modifying P_t .

Fixed quantities of interest for this work, inspired by Merritt et al. (2016) models of KS 1731-26, are the core temperature $T_c = 9.35 \times 10^7 \text{ K}$, accretion outburst duration $\Delta t_{\text{out}} = 12.5 \text{ yr}$, accretion rate $\dot{M} = 10^{17} \text{ g s}^{-1}$, accretion-driven shallow heating $\mathcal{H}_{\text{sh}} = 1.36 \text{ MeV}^{-1}$, shallow heating pressure boundaries $P_{\text{sh,low}} = 10^{27} \text{ g cm}^{-1} \text{ s}^{-2}$ and $P_{\text{sh,hi}} = 10^{28} \text{ g cm}^{-1} \text{ s}^{-2}$, low density boundary of the deep crustal heating $P_{\text{deep,low}} = 10^{30.42} \text{ g cm}^{-1} \text{ s}^{-2}$, light element atmosphere column depth $y_{\text{lite}} = 10^4 \text{ g cm}^{-2}$, neutron star core mass $M_c = 1.4 M_\odot - M_{\text{crust}}$ and radius (core radius plus crust thickness) $R = R_c + \Delta r = 12.31 \text{ km}$, crust pressure boundaries $P_{\text{cr,top}} = 10^{27.2} \text{ g cm}^{-1} \text{ s}^{-2}$ and

$P_{\text{cr,bot}} \equiv P_t$, and crust impurity $Q_{\text{imp}} = 4$. In general, Q_{imp} varies throughout the crust (Lau et al. 2018), but we choose a single value for the entire crust. This is partly to simplify the analysis, but the main justification is that the inner crust Q_{imp} has the dominant impact on τ and it is unlikely to vary substantially in this region (see Section 1).

As changes in P_t largely change the depth that the crust extends down to, we also investigate the impact of modified P_t when making various assumptions about deep crustal heat release $\mathcal{H}_{\text{deep}}$, the high-density boundary of the deep crustal heating $P_{\text{deep,hi}}$ (here assumed to be equal to P_t)³, and the neutron superfluid gap, which ultimately determines K near the base of the crust (Deibel et al. 2017).

Figure 1 shows example cooling curves, with data for KS 1731-26 (Merritt et al. 2016) included for comparison, highlighting the impact of varying EoS related properties M , R , and P_t . The X-ray flux is described by the effective temperature for an observer at infinite distance $k_B T_{\text{eff}}^\infty = (1+z)k_B T_{\text{surf}}$, where k_B is the Boltzmann constant and T_{surf} is the local surface temperature, as is customary for the corresponding observational data. The general trend is due to the heat deposited from nuclear processes in the deep crust reaching the surface at later times, relative to shallower layers, until crust-core equilibrium is achieved (e.g., at several thousand days in Figure 1). Smaller R for fixed M corresponds to larger $(1+z)$, stretching the cooling curve in time. The same is true for larger M at a fixed R . A larger P_t implies a thicker Δr , which one would naively associate with a longer cooling time for a fixed M, R . We see, however, no such impact, which we explain in the following section.

To test if the insensitivity depended on assumptions of properties near the crust-core transition, we investigated the impact of varying P_t when adopting different $\mathcal{H}_{\text{deep}}$ and models of the neutron singlet pairing gap. The impact of pairing gap models primarily relates to whether or not the neutron singlet pairing gap closes in the inner crust or in the core (Deibel et al. 2017). Figure 2 shows the impact of neutron singlet models CCDK93 (Chen et al. 1993), GC (Gezerlis & Carlson 2008; Takatsuka 1972), GIPSF08 (Gandolfi et al. 2008) with the gap closing at Fermi momentum $k_F = 1.1 \text{ fm}^{-1}$, GIPSF08-2 at $k_F = 1.3 \text{ fm}^{-1}$, GIPSF0-3 at $k_F = 1.5 \text{ fm}^{-1}$, SFB03 (Schwenk et al. 2003), and WAP (Wambach et al. 1993). Figure 3 shows the impact of varied $\mathcal{H}_{\text{deep}}$, choosing the extreme cases featured in Steiner (2012).

4. DISCUSSION

³ It is likely that deep heating is concentrated at densities just greater than neutron-drip (Zdunik et al. 2017), but we choose to extend it to the base of the crust in order to maximize the potential impact of modifying P_t .

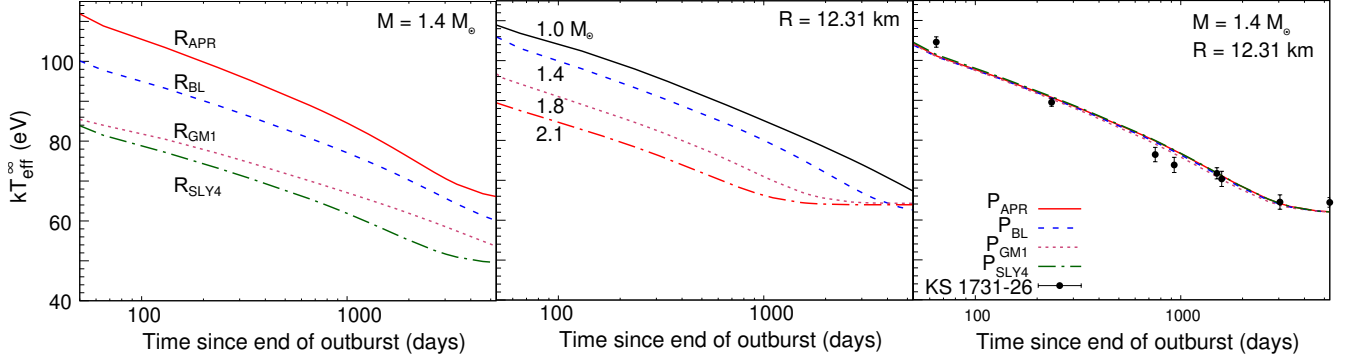


Figure 1. Impact of varied R , M , or P_t on crust cooling when the other two properties are fixed. The left and right panels use R and P_t , respectively, consistent with the EoS (see Table 1). The left and center panels use an arbitrary fixed P_t .

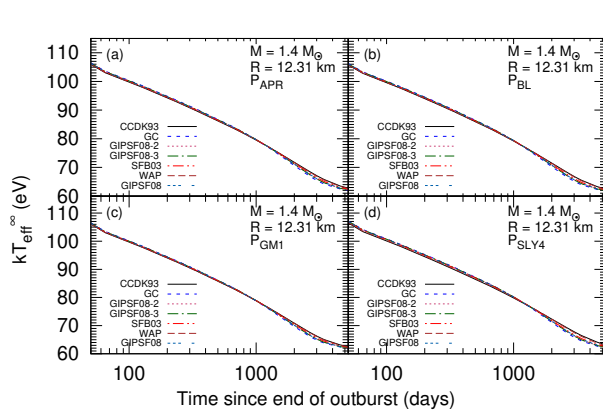


Figure 2. Impact of varied neutron singlet pairing gaps on crust cooling when using P_t according to various EoS.

We find a negligible impact on the crust cooling light curve, despite Δr changing nearly 20% over the range of P_t explored here. This counterintuitive result can be understood by considering the information the crust cooling light curve communicates about the crust thermal structure and the return of the thermal structure to equilibrium after accretion turnoff.

The X-ray luminosity emitted from the cooling transient source depends on the surface temperature at the time of emission. Sustained accretion results in a thermal structure that primarily decreases in temperature with increasing depth. As such, the surface cools to reach thermal equilibrium with continuously deeper depths as time progresses after accretion turnoff. Meanwhile, a large amount of heat diffuses into the relatively cold neutron star core. Therefore, by the time the cooling wave from the surface reaches the depths near P_t , these regions have already nearly become isothermal with the core (see, e.g., Page & Reddy 2013, Fig. 3). This means that the extra crust thickness acquired from increasing P_t is essentially invisible. Figure 4 demonstrates this for the calculations presented in this work, featuring the thermal

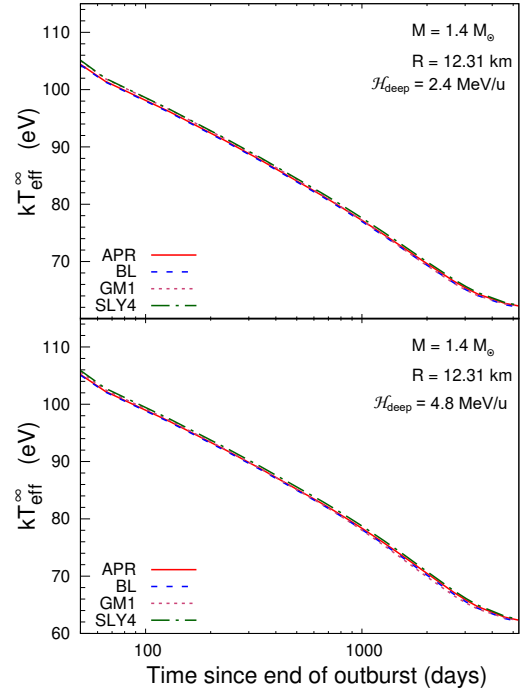


Figure 3. Impact of varied $\mathcal{H}_{\text{deep}}$ on crust cooling when using P_t according to various EoS.

profiles for the case modeled in the bottom panel of Figure 3, just after accretion turn-off and 1500 days into cooling. For the latter set of profiles, it is evident that the surface is in equilibrium with pressures much lower than P_t , while the region near P_t is nearly indistinguishable regardless which EoS is adopted.

For increased Q_{imp} , the inner crust will take longer to cool into thermal equilibrium with its surroundings and therefore the thermal structure at accretion turn-off will be maintained longer. Figure 5 demonstrates that sensitivity to P_t begins to set-in for $Q_{\text{imp}} = 25$, though differences between model results are still well within observational uncertainties. For context, $Q_{\text{imp}} \approx 20$ was found in the inner crust by Lau

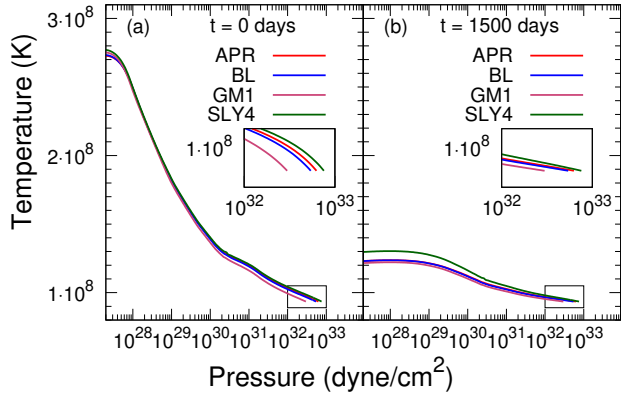


Figure 4. Thermal profiles for *dStar* calculations corresponding to the bottom panel of Figure 3 at accretion turnoff (a) and 1500 days later (b).

et al. (2018) using crust reaction network calculations for an exceptionally hydrogen-rich X-ray bursting system. This was the largest Q_{imp} found in that work for the inner crust.

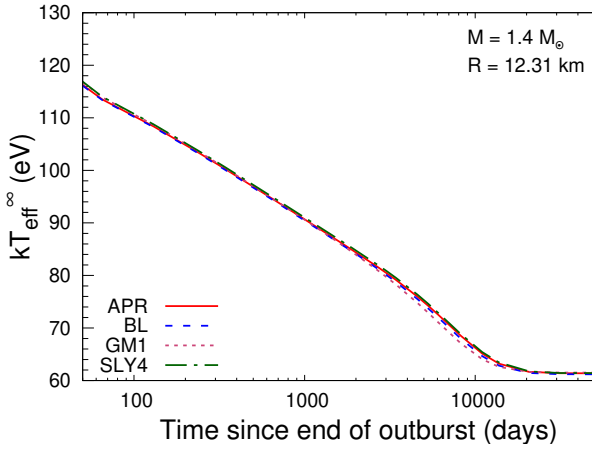


Figure 5. Impact of adopting P_t from various EoS for $Q_{\text{imp}} = 25$.

The insensitivity to P_t significantly simplifies the task of modeling crust cooling for observed cooling transient sources. This is because M and R can be arbitrarily selected without the need to assume an EoS in order to consistently calculate P_t . Additionally, the discrepancy in P_t between different procedures to match the EoS at the crust-core interface (Fortin *et al.* 2016; Gonzalez-Boquera *et al.* 2019) is unlikely to impact results for crust cooling models. Therefore, from this perspective, the use of a consistent EoS for the core and crust is not essential.

Thus far we have restricted ourselves to realistic EoS. One might wonder how far outside of the range in Table 1 that P_t would have to be in order to result in an observable impact.

This is addressed by Figure 6. Relative to observational uncertainties (see Figure 1), a significant impact would require roughly 0.5 dex increase (decrease) above (below) the largest (smallest) P_t in Table 1.

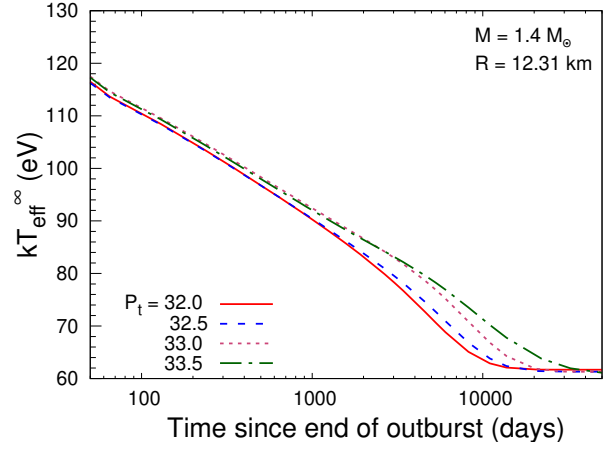


Figure 6. Impact of adopting arbitrary P_t for $Q_{\text{imp}} = 25$.

5. CONCLUSIONS

In summary, we investigated the impact of the P_t on the light curves of cooling transient sources as calculated via crust cooling models. Using *dStar* models and conditions resembling those that reproduce observations of the source KS 1731-26, we show model results are insensitive to P_t when adopting pressures corresponding to realistic EoS. We find this is because the region near the crust-core interface reaches thermal equilibrium with the core long before the surface cools into equilibrium with these depths. This finding justifies the previously adopted approach in model-observation comparisons of neutron star crust cooling where M and R are varied irrespective of considering an EoS to determine a consistent P_t . This also mitigates concerns about the dependence of P_t on the procedure used to match EoS at the crust and core interface.

We thank Ryan Connolly for useful discussions and *CompOSE* (<https://compose.obspm.fr>) for providing EoS data. This work was supported by the U.S. Department of Energy under grants DE-FG02-93ER-40756, DE-FG02-88ER40387, and DESC0019042. EFB is supported by the US National Science Foundation grant AST-1812838. We benefited from support by the National Science Foundation under grant PHY-1430152 (Joint Institute for Nuclear Astrophysics–Center for the Evolution of the Elements).

Software: *dStar* (Brown 2015)

REFERENCES

- Akmal, A., Pandharipande, V. R., & Ravenhall, D. G. 1998, *PhRvC*, 58, 1804
- Antoniadis, J., Freire, P. C. C., Wex, N., et al. 2013, *Science*, 340, 448
- Baym, G., Hatsuda, T., Kojo, T., et al. 2018, *RPPH*, 81, 056902
- Bombaci, Ignazio, & Logoteta, Domenico. 2018, *A&A*, 609, A128
- Brown, E., & Cumming, A. 2009, *ApJ*, 698, 1020
- Brown, E. F. 2015, *Astrophysics Source Code Library*, ascl:1505.034
- Brown, E. F., Bildsten, L., & Rutledge, R. E. 1998, *ApJL*, 504, L95
- Chabanat, E., Bonche, P., Haensel, P., Meyer, J., & Schaeffer, R. 1998, *NuPhA*, 635, 231
- Chen, J., Clark, J., Davé, R., & Khodel, V. 1993, *NuPhA*, 555, 59
- Colpi, M., Geppert, U., Page, D., & Possenti, A. 2001, *ApJL*, 548, L175
- Degenaar, N., Medin, Z., Cumming, A., et al. 2014, *ApJ*, 791, 47
- Degenaar, N., Wijnands, R., Bahramian, A., et al. 2015, *MNRAS*, 451, 2071
- Deibel, A., Cumming, A., Brown, E. F., & Page, D. 2015, *ApJL*, 809, L31
- Deibel, A., Cumming, A., Brown, E. F., & Reddy, S. 2017, *ApJ*, 839, 95
- Demorest, P. B., Pennucci, T., Ransom, S. M., Roberts, M. S. E., & Hessels, J. W. T. 2010, *Nature*, 467, 1081
- Douchin, F., & Haensel, P. 2001, *A&A*, 380, 151
- Fortin, M., Providência, C., Raduta, A. R., et al. 2016, *PhRvC*, 94, 035804
- Gandolfi, S., Illarionov, A. Y., Fantoni, S., Pederiva, F., & Schmidt, K. E. 2008, *PhRvL*, 101, 132501
- Gezerlis, A., & Carlson, J. 2008, *PhRvC*, 77, 032801
- Glendenning, N. K., & Moszkowski, S. A. 1991, *PhRvL*, 67, 2414
- Gonzalez-Boquera, C., Centelles, M., Viñas, X., & Routray, T. R. 2019, *arXiv e-prints*, arXiv:1904.06566
- Gulminelli, F., & Raduta, A. R. 2015, *PhRvC*, 92, 055803
- Gupta, S., Brown, E. F., Schatz, H., Moller, P., & Kratz, K.-L. 2007, *ApJ*, 662, 1188
- Heney, L., & L'Ecuyer, J. 1969, *ApJ*, 156, 549
- Horowitz, C. J., Brown, E. F., Kim, Y., et al. 2014, *Journal of Physics G Nuclear Physics*, 41, 093001
- Itoh, N., & Kohyama, Y. 1993, *ApJ*, 404, 268
- Lalit, S., Mamun, M. A. A., Constantinou, C., & Prakash, M. 2019, *European Physical Journal A*, 55, 10
- Lattimer, J. M. 2012, *ARNPS*, 62, 485
- Lattimer, J. M., & Prakash, M. 2016, *Physics Reports*, 621, 127
- Lau, R., Beard, M., Gupta, S. S., et al. 2018, *ApJ*, 859, 62
- Medin, Z., & Cumming, A. 2014, *ApJL*, 783, L3
- Meisel, Z., & Deibel, A. 2017, *ApJ*, 837, 73
- Meisel, Z., Deibel, A., Keek, L., Shternin, P., & Elfriz, J. 2018, *JPhG*, 45, 093001
- Merritt, R. L., Cackett, E. M., Brown, E. F., et al. 2016, *ApJ*, 833, 186
- Newton, W. G., Gearheart, M., & Li, B.-A. 2013, *ApJS*, 204, 9
- Ootes, L. S., Wijnands, R., Page, D., & Degenaar, N. 2018, *MNRAS*, 477, 2900
- Oppenheimer, J. R., & Volkoff, G. M. 1939, *PhRv*, 55, 374
- Özel, F., & Freire, P. 2016, *ARA&A*, 54, 401
- Page, D., & Reddy, S. 2013, *PhRvL*, 111, 241102
- Parikh, A. S., Wijnands, R., Degenaar, N., Ootes, L., & Page, D. 2018, *MNRAS*, 476, 2230
- Parikh, A. S., Homan, J., Wijnands, R., et al. 2017, *ApJL*, 851, L28
- Parikh, A. S., Wijnands, R., Ootes, L. S., et al. 2018, *arXiv e-prints*, arXiv:1810.05626
- Paxton, B., Bildsten, L., Dotter, A., et al. 2011, *ApJS*, 192, 3
- Paxton, B., Cantiello, M., Arras, P., et al. 2013, *ApJS*, 208, 4
- Paxton, B., Marchant, P., Schwab, J., et al. 2015, *ApJS*, 220, 15
- Paxton, B., Schwab, J., Bauer, E. B., et al. 2018, *ApJS*, 234, 34
- Rutledge, R. E., Bildsten, L., Brown, E. F., et al. 2002, *ApJ*, 580, 413
- Schwenk, A., Friman, B., & Brown, G. E. 2003, *NuPhA*, 713, 191
- Shternin, P. S., Yakovlev, D. G., Haensel, P., & Potekhin, A. Y. 2007, *MNRAS*, 382, L43
- Sotani, H., Iida, K., & Oyamatsu, K. 2017, *MNRAS*, 470, 4397
- Steiner, A. W. 2012, *PhRvC*, 85, 055804
- Steiner, A. W., Gandolfi, S., Fattoyev, F. J., & Newton, W. G. 2015, *PhRvC*, 91, 015804
- Takatsuka, T. 1972, *Prog. of Theor. Phys.*, 48, 1517
- Tolman, R. C. 1939, *PhRv*, 55, 364
- Tsaloukidis, L., Margaritis, C., & Moustakidis, C. C. 2019, *Phys. Rev. C*, 99, 015803
- Turlione, A., Aguilera, D. N., & Pons, J. A. 2015, *A&A*, 577, A5
- Ushomirsky, G., & Rutledge, R. E. 2001, *MNRAS*, 325, 1157
- Vats, S., Ootes, L. S., Wijnands, R., et al. 2018, *arXiv e-prints*, arXiv:1805.00610
- Wambach, J., Ainsworth, T., & Pines, D. 1993, *NuPhA*, 555, 128
- Waterhouse, A. C., Degenaar, N., Wijnands, R., et al. 2016, *MNRAS*, 456, 4001
- Wijnands, R., Degenaar, N., & Page, D. 2017, *JApA*, 38, 49
- Zdunik, J. L., Fortin, M., & Haensel, P. 2017, *A&A*, 599, A119